



OPEN

SUBJECT AREAS:

SCANNING PROBE
MICROSCOPY

IMAGING TECHNIQUES

IMAGING AND SENSING

CHARACTERIZATION AND
ANALYTICAL
TECHNIQUES

Quantitative Imaging of Rapidly Decaying Evanescent Fields Using Plasmonic Near-Field Scanning Optical Microscopy

Zhen Zhang^{1*}, Phillip Ahn^{1*}, Biqin Dong^{1*}, Oluwaseyi Balogun^{1,2} & Cheng Sun¹¹Mechanical Engineering Department, Northwestern University, Evanston, IL 60208, ²Civil and Environmental Engineering Department, Northwestern University, Evanston, IL 60208.Received
25 June 2013Accepted
11 September 2013Published
30 September 2013

Correspondence and requests for materials should be addressed to O.B. (o-balogun@northwestern.edu) or C.S. (c-sun@northwestern.edu)

* These authors contributed equally to this work.

Non-propagating evanescent fields play an important role in the development of nano-photonics devices. While detecting the evanescent fields in far-field can be accomplished by coupling it to the propagating waves, in practice they are measured in the presence of unwanted propagating background components. It leads to a poor signal-to-noise ratio and thus to errors in quantitative analysis of the local evanescent fields. Here we report on a plasmonic near-field scanning optical microscopy (p-NSOM) technique that incorporates a nanofocusing probe for adiabatic focusing of propagating surface plasmon polaritons at the probe apex, and for enhanced coupling of evanescent waves to the far-field. In addition, a harmonic demodulation technique is employed to suppress the contribution of the background. Our experimental results show strong evidence of background free near-field imaging using the new p-NSOM technique. Furthermore, we present measurements of surface plasmon cavity modes, and quantify their contributing sources using an analytical model.

Recent studies of surface plasmon polaritons (SPPs) have led to new opportunities for manipulating light at deep sub-wavelength length scales^{1–4}. SPPs are formed by coupling electromagnetic (EM) waves to the collective excitation of free carriers at the surface of a metal. Such surface-bound resonance modes have enabled various novel optical phenomena including: super-resolution optical imaging^{5–9}, nano-lithography^{10–12}, enhanced Raman scattering^{13–19}, and second harmonic generation^{20,21}.

Two distinguishing characteristics of SPPs are that for a given energy, the magnitude of the in-plane wavevector is usually larger than that of a light wave in free space, and the out-of-plane component of the wavevector is imaginary due to energy conservation. Consequently, the amplitude of SPPs decays exponentially with distance away from a sample surface like an evanescent wave. Quantitative analysis and mapping of SPPs would require high lateral spatial resolution and more importantly, the ability to detect non-propagating evanescent fields bound to a sample surface^{22–24}. This can be achieved by placing a small scattering center within the near-field of a sample to transform the evanescent fields to the propagating waves that can be collected in the far-field. As an example, near-field scanning optical microscopy (NSOM) is implemented by scanning a sub-wavelength metal or dielectric probe in the near-field of a sample. The probe-tip scatters the evanescent waves to the far-field, and the measured data carries information of the local optical properties of the sample^{25–28}. Since the operation of NSOM relies on conversion of evanescent fields to propagating waves, it becomes critical to distinguish between the overlapping information in the propagating wave channel, which may result from specular and diffuse light reflections from the shaft of the probe-tip and from the sample surface. The amplitude of these background reflections is substantially larger than that of the evanescent waves, and the background contributes to measurement artifacts in near-field optical images. A potential method to overcome the strong background scattering effects in NSOM is to couple free-space light to the SPPs that spatially focus at the apex of a probe-tip. With this approach, the optical scattering cross-section of the probe-tip and sample interaction is enhanced in comparison to the background. By utilizing localized plasmonic resonance, the detection sensitivity and spatial resolution of apertureless NSOM using sharp metallic tips^{29–31} or nano-particles³² have been improved in comparison to conventional apertured NSOM. However, due to the limited absorption cross-section, only a small portion of free-space light can be localized in the near-field of the particle probe. A more energy efficient approach is based



on coupling free-space light to the propagating SPPs, which allows for effective focusing of light at the apex of a probe-tip. Various schemes have been developed for plasmonic nanofocusing including prism couplers³³, diffraction gratings^{34,35}, circularly symmetric waveguides, or tapered structures that adiabatically convert propagating modes into localized SPPs at apex of structures such as cones^{36,37} and wedges^{38,39}. Recently, plasmonic focusing on a scanning tunneling microscopy probe was experimentally demonstrated with strong evidence of local field enhancement at the probe-tip^{40–44}. This development paved the way for integration of nanofocusing devices with scanning probe microscopy techniques. Plasmonic nanolithography³⁵, which utilizes metallic structures can also benefit from optical field enhancement provided by adiabatic SPP focusing structures. In this case, propagating SPPs are favorable for energy transfer over long distances and localized SPPs can provide intense optical field confinement needed for material structuring or patterning. However, in practice, the presence of SPP propagation losses arising from conversion of electromagnetic energy to heat and scattering from surface roughness limits the strength of nanofocused SPPs. In the context of scanning probe microscopy, these propagation losses limit the intensity of the local evanescent waves coupled to the far-field as compared to the background. Consequently, in order to achieve background-free measurement of the local evanescent field, one may require the use of modulation techniques commonly used in scattering type NSOM⁴⁵.

In this work, we describe a new NSOM system that incorporates two key building blocks: 1) a hybrid plasmonic nanofocusing probe for adiabatically converting propagating SPPs into localized modes at apex of a metallic probe-tip to improve the coupling efficiency of evanescent to propagating waves⁴⁶, and 2) a modulation technique to suppress the background modes in the propagating wave channel. We demonstrate sub-wavelength background-free imaging of local plasmonic fields. Using basic analytical modeling, we quantify the relative strengths of SPPs coupled to a sample from the probe-tip, and background evanescent modes excited by diffraction of free-space light from metal discontinuities. We also explore the technique for analyzing complicated SPP interference patterns formed in a plasmonic cavity.

Results

Experimental setup and methodology. Figure 1 shows a schematic of the plasmonic nanofocusing probe. The probe uses design elements from a hybrid nanofocusing technique recently developed for high-speed nanolithography⁴⁷ and for near-field optical microscopy^{34,43}. In the figure, long-range SPPs are excited by focusing far-field light onto a diffraction grating patterned on the shaft of a metallic probe. The SPPs propagate towards the probe-tip where they are localized into a bright nanoscale optical source. In this work, a coherent *p*-polarized frequency doubled neodymium yttrium aluminum garnet (Nd:YAG) laser with a wavelength of 532 nm is used as a free-space light source. The plasmonic nanofocusing probe is fabricated from a commercial silicon atomic force microscope (AFM) scanning probe. The *as-received* AFM probe has a nominal tip radius of 10 nm and is supported by a flexure mode silicon cantilever. The probe is coated with a 200 nm thick silver film and a one-dimensional SPP coupling grating is fabricated on its front facets by focused ion beam (FIB) milling. Figure 1(b) shows scanning electron microscopy (SEM) images of the AFM probe and the coupling grating. The probe-tip radius after depositing the silver film is less than 30 nm. The first order diffraction of the grating provides the momentum needed to couple the incident light to SPPs, such that, $k_{sp} = k_0 \sin \alpha \pm 2\pi/\Delta$, where $k_0 = 2\pi/\lambda$ is the wavenumber of the light source, k_{sp} is the SPP wavenumber, $\lambda = 532$ nm is the wavelength of the illumination source, Δ is the grating period, and $\alpha = 15^\circ$ is the angle between illumination wave vector and the normal line from the ridge on the

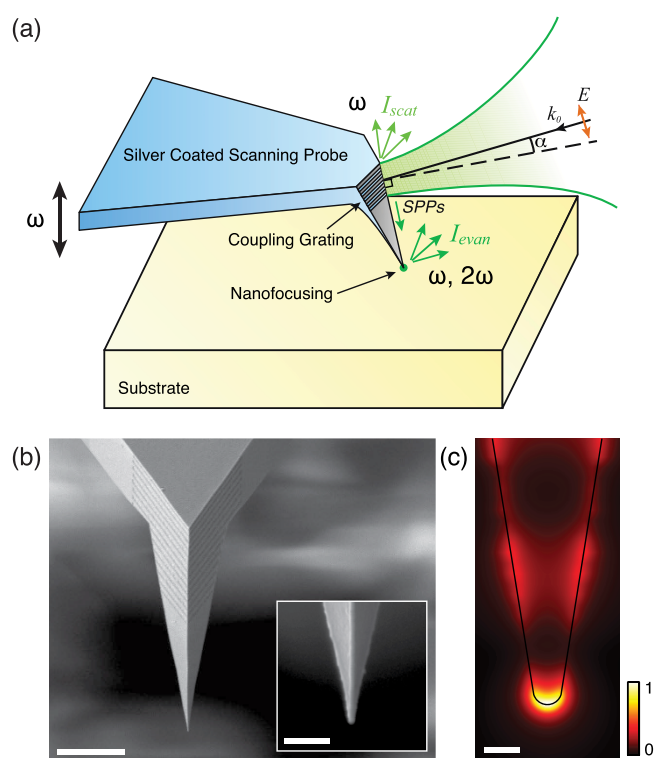


Figure 1 | (a) Schematic illustration of the working principle of the hybrid nanofocusing of SPPs and detection of weak optical near-field. (b) Top-view of the hybrid nanofocusing probe obtained with a scanning electron microscope. Scale bar in figure is 5 μm . Insert in figure shows the probe-tip. Scale bar in insert is 500 nm. (c) FDTD numerical simulation of adiabatic nanofocusing shows local electric field intensity distribution. Scale bar is 50 nm.

AFM probe. There is another angle φ not illustrated in the figure, between the surface normal to the facets and normal line to the ridge. The coupling (or diffraction) efficiency of the illumination source to SPPs is proportional to $\cos\varphi$, but does not depend on the spatial periodicity of the grating. The grating is designed for excitation of SPPs using direct optical illumination through air and Δ is equal to 669 nm. The insert in Fig. 1(b) shows a close up view of the probe-tip. The excited SPPs propagate along the tapered surface of the AFM probe and are focused at the probe-tip. Figure 1(c) shows a cross-section image of a three-dimensional finite-difference time domain (FDTD) simulation of SPP focusing at the apex of a triangular silver probe having a tip radius of 20 nm. SPPs are launched on the facets of the probe and propagate to the probe-tip. The numerical result shows the electric field confinement at the tip apex, where the intensity of the local SPPs is enhanced by two orders of magnitude.

The plasmonic nanofocusing probe is incorporated into a home-built NSOM system shown schematically in Fig. 2. The setup uses a commercial AFM system (INNOVA™ AFM from Bruker) for scanning the probe-tip in close proximity to the sample. The cantilever probe is vibrated at its fundamental tapping mode resonance frequency ω of 330 kHz with an amplitude of ~ 20 nm, and the AFM system maintains the average separation distance between the probe and the sample surface using a closed-loop feedback system. The AFM cantilever vibration was confirmed using an optical interferometer. The illumination laser is focused on the AFM probe through a 10x microscope objective with a numerical aperture of 0.35. A portion of the light reflected from the AFM cantilever shaft and sample creates background propagating waves that are collected in the far-field. The background contributions are suppressed using modulation techniques^{48,49}. The tapping motion of the AFM cantilever

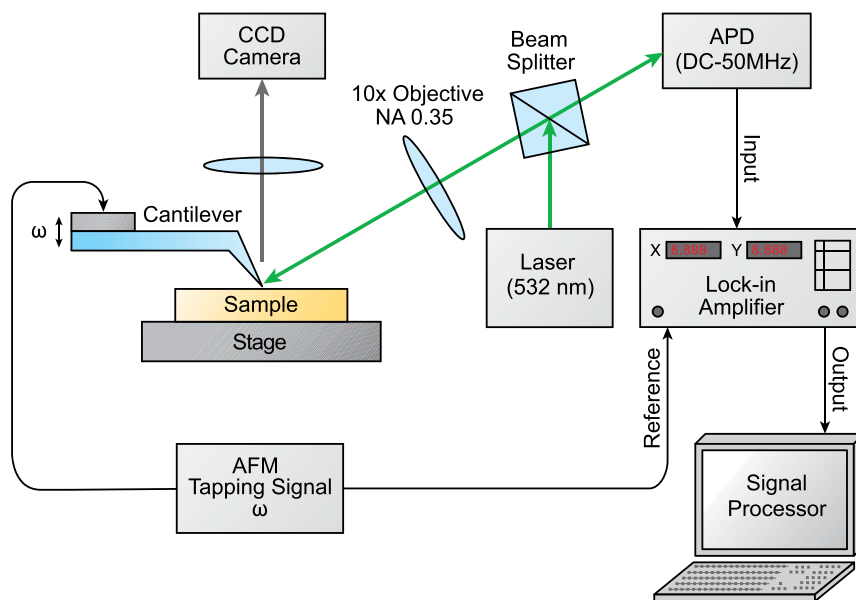


Figure 2 | Schematic of the experimental setup.

leads to the modulation of the collected light intensity. The optical scattering cross-section of the near-field probe has a nonlinear dependence on the separation distance between the probe-tip and the sample, particularly for distances comparable to the AFM tip radius a ($a \ll \lambda$, where λ is the wavelength of the illumination source). As such, the intensity of the near-field is temporally modulated at the AFM tapping mode frequency ω and its higher harmonic frequencies $n\omega$ ($n = 2, 3, 4$, etc.) by the motion of the probe-tip. In contrast, the background varies linearly over a short tip-sample separation distance that is much smaller than λ . The background is suppressed by demodulating the light intensity collected in the far-field at harmonics of ω , while the tip-sample distance changes between 0 and 40 nm, which is small as compared to the wavelength of the light⁵⁰. In the experimental setup, the collected light is delivered to an avalanche photodiode (APD110A, THORLABS) with a 50 MHz bandwidth and the electrical output voltage from the detector is demodulated in a radio frequency (RF) lock-in amplifier (SR844, SRS). The lock-in amplifier is operated with a time constant of 1 ms and it uses an input reference obtained by sampling a portion of the oscillating electrical voltage that drives the AFM cantilever.

Modulation techniques-approach curves. Figure 3 shows the amplitude of the collected light demodulated at ω and 2ω as the oscillating plasmonic nanofocusing probe approaches the sample. In the measurement, the AFM feedback was turned off, and the distance between the probe-tip and sample was varied by moving the sample stage towards the probe-tip. The sample consists of a 200 nm thick polycrystalline silver film on a silicon substrate. The zero distance position in the figure corresponds to the point where the oscillation amplitude of the AFM cantilever is equal to the average probe tip-sample separation distance. The data demodulated at ω shows a moderate change over small distances, and exhibits cyclic variation over a distance that is close to half the wavelength of the incident light. The intensity modulation is due to interference of background propagating light scattering from the sides of the AFM cantilever and the sample surface. In contrast, the measured data at 2ω exhibits a sharp decrease to the noise floor over a short distance, which resembles the exponential decaying characteristic of the evanescent fields surrounding the probe-tip. The sharp drop-off in the measured data within 6 nm in the inset of Fig. 3 results from destructive interference between the background and

near-field light. This hypothesis is confirmed using an analytical model for dynamic approach curves expected in an apertureless NSOM experiment⁵¹. In the model the phase difference between the background and near-field is assumed to be 0° and 180° for the case of destructive and constructive interference between the two sources. The model fits the measured data for the case where the phase difference is 180° , and the near-field is 1.8 times larger than the background. The near-field decay length is estimated to be approximately 10 nm based on the model. The approach curves demonstrate that use of modulation techniques result in successful suppression of the background through demodulation of the collected light at 2ω .

Near-field optical imaging with p-NSOM. To explore the influence of optical field enhancement on the near-field-to-background intensity ratio, we performed experiments on near-field imaging of patterned vanadium structures on a quartz substrate using two different probes, a silver coated AFM probe without the SPP

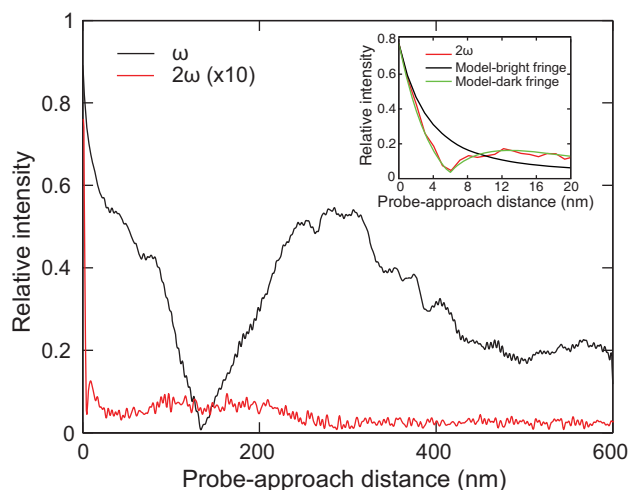


Figure 3 | Approach curves for the plasmonic nanofocusing probe demodulated at ω and 2ω showing the measured optical intensity as the probe approaches the sample. The inset shows the sharp drop-off of optical intensity demodulated at 2ω and its analytical fitting.



coupling gratings and the plasmonic nanofocusing probe. The vanadium film provides a suitable platform for pure near-field optical imaging since it does not support SPPs at the frequency of the illumination source. In the silver coated probe, localized SPPs can be excited near the apex of the silver tip. The plasmonic nanofocusing probe provides additional enhancement due to adiabatic focusing of the grating excited SPPs at the probe-tip. In the experiment, a part of the sample was imaged by demodulating the collected light at ω and 2ω . The thickness of the vanadium pattern is approximately 60 nm and the scan area on the sample is $10\ \mu\text{m} \times 10\ \mu\text{m}$. The power of free-space light illuminating the probe was limited to 0.5 mW in both experiments in order to prevent ablation of the metal film at the probe-tip due to heating caused by absorption of the tip localized SPPs. The measured optical images are compared to the sample topography in figure 4. The upper portion of each of the optical images is demodulated at ω , and the lower portions are demodulated data at 2ω . The data in Fig. 4(b) obtained at ω with the silver probe show fringes in the light intensity due to interference between far-field reflections from the sample and the AFM cantilever. The near-field optical images obtained with the plasmonic nanofocusing probe (Fig. 4(d)) show significantly weaker fringes in the ω data, completely suppressed fringes in the 2ω data, and a larger intensity contrast between vanadium and the quartz substrate. Using the harmonic (2ω) images, Figs. 4(b) & (d) provide intensity contrasts of 1.9 and of 2.3, respectively. We calculated the ratio of the optical scattering cross-section of vanadium and quartz to be approximately 2.6 using the quasi-static dipole model⁵⁰, which is close to the measured intensity contrast in Fig. 4(d). Furthermore, comparing Fig. 4(d) to (b), one

can observe qualitatively that larger near-field intensities are obtained with the plasmonic nanofocusing probe due to stronger scattering of localized SPPs at probe-tip to the far-field by the vanadium film. Suppose one defines the signal-to-noise ratio (SNR) in the 2ω images as a ratio of the mean intensity on the vanadium to the standard deviation, we obtain a SNR of 1.57 for Fig. 4(b) and 7.16 for Fig. 4(d). These numbers suggest that the plasmonic nanofocusing increases the near-field intensity compared to the background, which leads to high sensitivity to local optical properties.

Near-field optical imaging of local SPP modes. Using the plasmonic nanofocusing probe, we mapped the amplitude of localized SPPs on a 300 nm thick silver film deposited on a fused silica substrate. The objective of this experiment is to demonstrate quantitative mapping of local evanescent fields on the sample. The sample consists of a straight slit that is $10\ \mu\text{m}$ long and 200 nm wide, etched into the silver film by focused ion beam milling. The optical paths of all optical sources in the experiment are illustrated in Figure 5(a). When the probe-tip is close to the slit, the incident light illuminates the sharp edge of the slit in the silver film and diffracts, leading to the excitation of SPPs on the sample. In addition, the localized SPPs at the tip of the nanofocusing probe couple to SPP modes at the air/silver interface. The illumination angle θ with respect to the sample surface is approximately 18° . Figures 5(b) & (c) show the topography and near-field optical images obtained by scanning the sample and recording the intensity of the collected light at 2ω . The arrows in the NSOM images indicate the illumination direction. In the optical image of the straight slit, fringes with spatial wavelengths of approximately

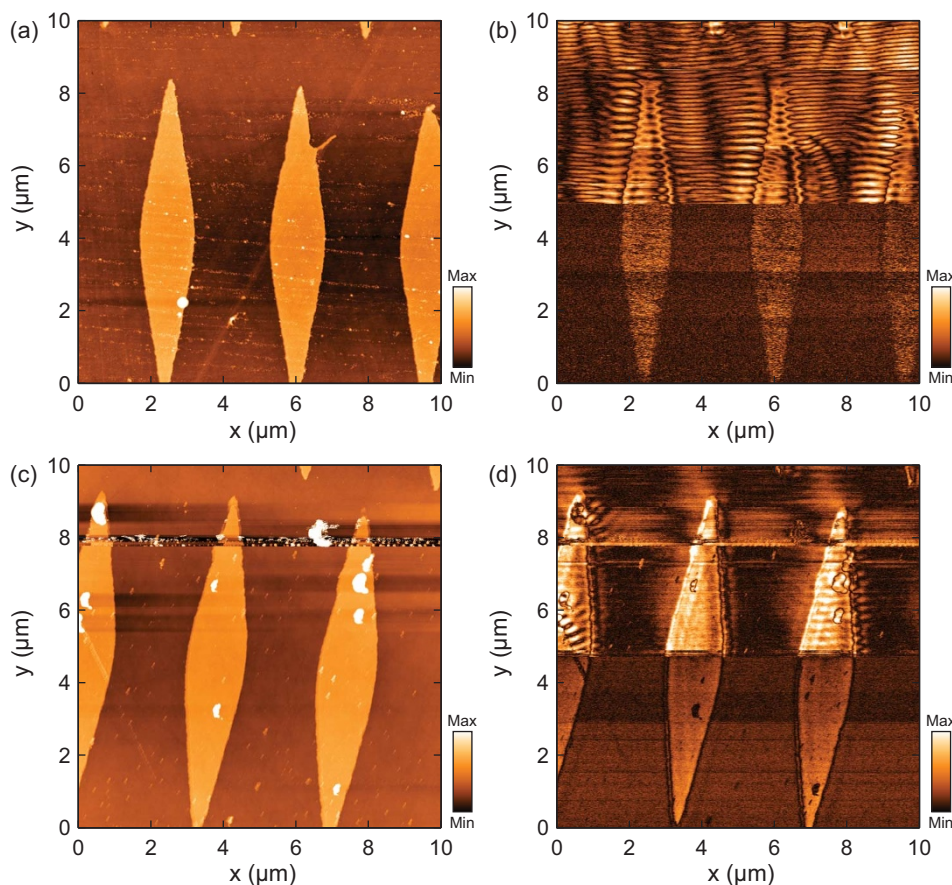


Figure 4 | Near-field optical images of patterned vanadium structures on a quartz substrate. Images show (a) topography and (b) near-field images obtained using a silver coated silicon probe without the SPP coupling gratings, and (c) topography and (d) near-field images obtained with the plasmonic nanofocusing probe. The upper parts of (b) and (d) are demodulated at ω , and the lower parts of the figures are demodulated at 2ω .

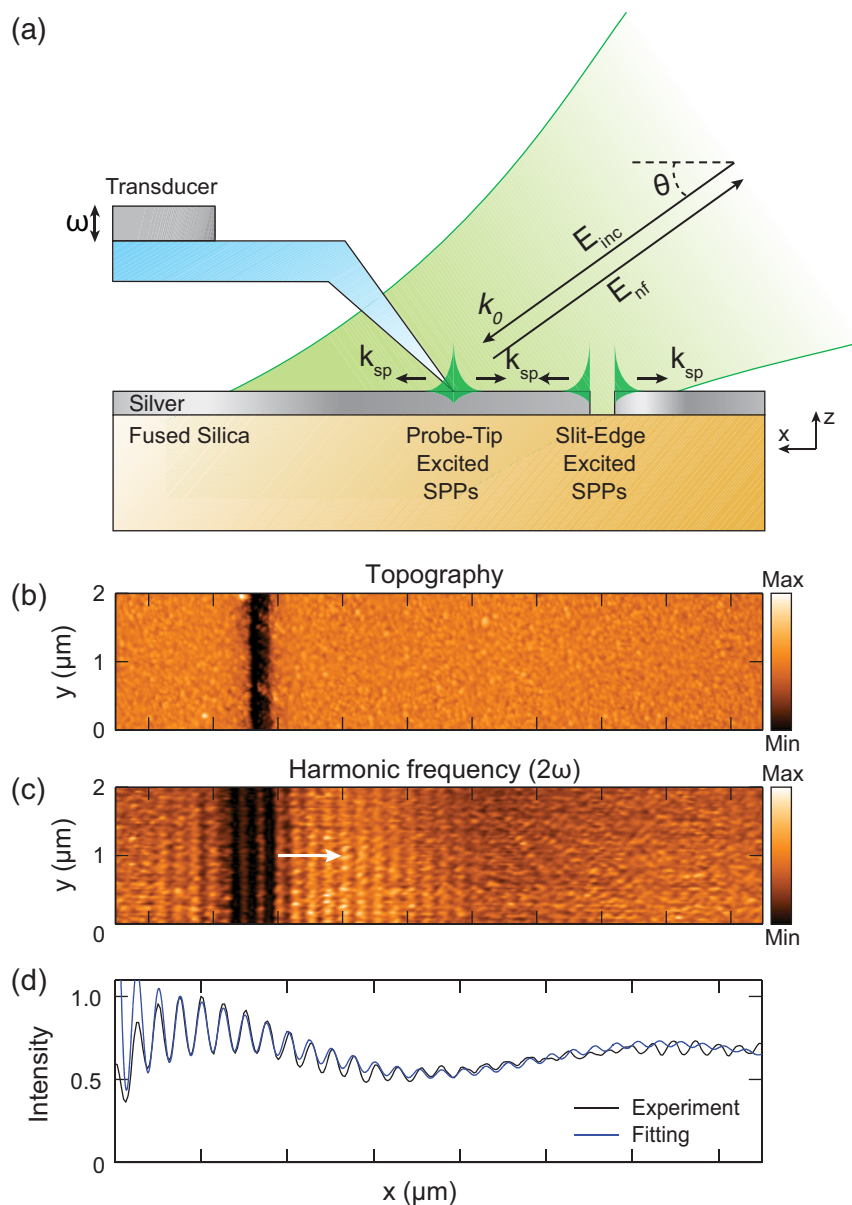


Figure 5 | (a) Excitation of SPPs on a silver film using the combination of a fabricated slit and localized SPPs at the probe-tip. The illumination angle $\theta = 18^\circ$. Images of a straight slit on a silver film showing (b) the AFM topography, and (c) near-field optical image recorded at 2ω . The average line trace of the near-field intensity in (c) is compared to an analytical model in (d).

5.25 μm and 253 nm are observed. The fringes are not due to interference of background reflections, but are produced by interference between the SPPs modes and the in-plane component of the incident light on the sample. Using a ray tracing based analytical model described in the Methods section, the relative intensity of the local interfering components are calculated and compared to the experimental data. To reduce the incoherent intensity noise in the measured data, line traces in Fig. 5(c) are averaged respectively to yield a plot of the mean intensity as a function of the spatial coordinate x . The analytical model yields a best fit to the averaged data using the following free parameters, $E_1/E_0 = 0.4$ and $E_2/E_0 = 18.0$ in a least-square fitting algorithm. The parameters E_1/E_0 , E_2/E_0 represent the relative amplitudes of the slit-edge excited SPPs and the probe-tip excited SPPs being normalized by that of the incident light. The fitted results suggest that the intensity of the SPPs excited by the probe-tip is larger than the slit-edge due to the combination of higher coupling efficiency provided by the grating and adiabatic nanofocusing of SPPs at the

probe-tip. The analytical model is in good agreement with the experimental data and the expected intensity oscillations are clearly observed. Using the model, we confirmed that these oscillations are due to interference between, (1) the slit-edge excited SPPs and the projection of the incident light in the forward direction (or positive x direction), which leads to slow intensity oscillations with a spatial period of $2\pi/(k_{sp,x} - k_0 \cos\theta) = 5.25 \mu\text{m}$, with $k_{sp,x}$ and k_0 being the wavenumbers of the in-plane SPPs on the metal film and the incident light, (2) the phase retarded probe-tip excited SPPs and the incident light, producing fast oscillations with a period of $\pi/k_{sp,x} = 253 \text{ nm}$, and (3) the slit-edge excited SPPs and the phase retarded probe-tip excited SPPs, producing fast oscillations with a period of $2\pi/(3k_{sp,x} - k_0 \cos\theta) = 241 \text{ nm}$. The intensity of the fast oscillations decreases with distance from the slit-edge due to a combination of geometric attenuation and intrinsic damping of the SPP mode. Since the propagation length of the SPPs is $\delta_{SP} = 1/k''_{sp,x} = 9.167 \mu\text{m}$ at the frequency of the light source ($k''_{sp,x}$ is the imaginary part of $k_{sp,x}$), which is much longer than the observed



decay length in the data, it is reasonable to conclude that the amplitude decay is dominated by geometric attenuation. It is noteworthy to mention that the intensity oscillations ride over a large DC intensity level that effectively reduces the modulation depth. The DC intensity is not due to the background scattering, but results from the interference terms detailed by Eqn. 3 in the Methods section.

Using the normalized field amplitude obtained from the experiment, we further explored the plasmonic probe for quantitative imaging of localized polariton modes within an SPP cavity in the silver film. In the experiment, the nanofocusing probe couples SPPs to a circular ring with a diameter of 5 μm . Figure 6(a) shows the topography of the ring and the corresponding near-field image demodulated at 2ω is shown in Figure 6(b). A more complicated fringe pattern is observed in the measured data as compared to the straight slit due to the geometry of the ring. A related interference structure was observed using surface phonon polaritons at infrared frequencies by Huber *et al.*^{48,49}. In order to interpret the sources of the fringes using the analytical model, we calculated the fringe pattern resulting from interference between, (1) the in-plane projection of the incident light, (2) the probe-tip excited SPPs coupled to the sample surface, and (3) the slit-edge excited SPPs inside and around the ring. These results are plotted in Figs. 6(c–e). For these calculations, the slit-edge excited SPPs are modeled by a distribution of point dipoles around the circumference of the ring, and the field amplitude ratios of different sources obtained from the fitting parameters in the slit experiment are assumed. In Fig. 6(c), fringes generated by interference between slit-edge excited SPPs and the projection of the illumination source are observed in and around the ring. The arrow in the near-field image indicates the illumination direction. The wavelength of the fringes resulting from interference between the forward propagating ring-edge excited SPPs and the illumination source is $2\pi/(k_{sp,x} - k_0\cos\theta) = 5.25 \mu\text{m}$, which is seen as the low spatial frequency fringes inside and around the upper

portion of the ring. In addition, fringes resulting from interference between the backward propagating ring-edge excited SPPs and the illumination source, having a period of $2\pi/(k_{sp,x} + k_0\cos\theta) = 265 \text{ nm}$, are observed around the lower portion of the ring in Fig. 6(c). In Fig. 6(d), the probe-tip excited SPPs inside the ring coupling to the silver surface propagate outwards with circular wavefronts, reflect from the edges, and focus at the center location, producing a pattern of concentric interference fringes with respect to the center of the ring. The period of the interference fringes is $\pi/k_{sp,x} = 253 \text{ nm}$. Figure 6(e) shows a combination of these wave interference patterns, which are seen to be in good agreement with the measured data. These experiments clearly demonstrate the potential of the plasmonic near-field optical microscopy system for quantitative imaging of decaying evanescent fields in optically excited structures.

Discussion

In conclusion, we have explored adiabatic nanofocusing for localizing SPPs at the apex of a scanning probe. We showed that the approach enhances the intensity of the SPPs and produces a bright near-field optical source, and background reflections from the sample and probe cantilever while still present are diminished in comparison to the localized SPPs. The background are eliminated using traditional modulation techniques. We demonstrated that the probe serves as a local near-field optical source and detector for quantitative analysis of the rapidly decaying SPP fields on a sample. The p-NSOM system has several advantages including the ease of probe manufacturing and small optical interaction volume compared with aperture type NSOM, which can lead to improved imaging contrast and spatial resolution in optical microscopy. In the future, combining interferometric techniques with the NSOM detection would enable simultaneous measurement of the amplitude and phase of evanescent optical waves. The strong coupling of localized SPPs from the nanofocusing probe to the sample observed in the measured data may hold great

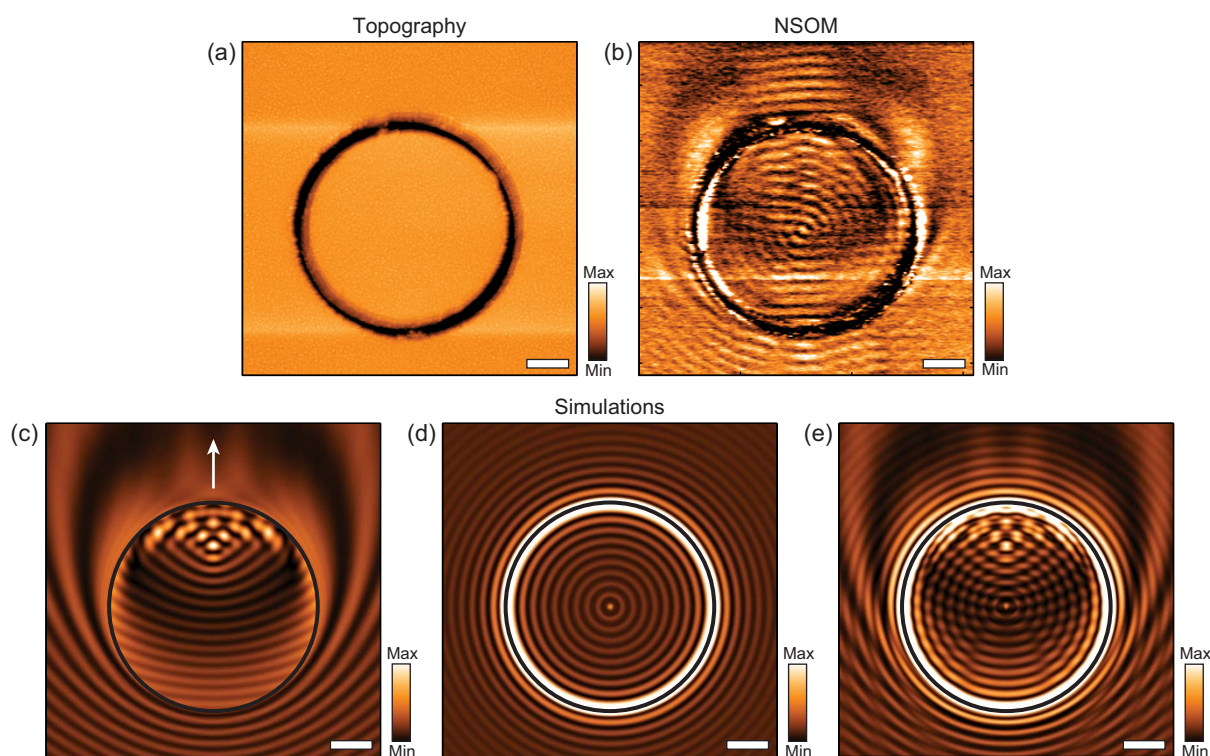


Figure 6 | Images of a circular plasmonic cavity on a silver film surface showing (a) the measured AFM topography, and (b) near-field optical image demodulated at 2ω . Numerical results of the interference pattern formed between, (c) the illumination source and the slit-edge excited SPPs, (d) the reflected probe-tip excited SPPs, and (e) the combination of the illumination and all SPP sources. Scale bar in figure is 1 μm .



potential for local control of optical and opto-thermal stimulated processes in nanoscale structures.

Methods

Experimental details. The plasmonic nanofocusing probe was fabricated from a commercially available AFM probe (VIT_P, NT-MDT). The probe geometry allows easy access for direct coupling of far-field light to propagating SPPs through the diffraction grating, and a large collection numerical aperture for far-field detection.

Analytical details. In order to analyze the measured intensity data quantitatively, we model the total electric field at a given position (x, z) of the probe as,

$$E_p(x, z) = E_i(x, z) + E_{sp_edge}(x, z) + E_{sp_probe}(x, z), \quad (1)$$

where the subscripts i , sp_edge , and sp_probe stand for the projection of the illumination source in the forward propagation direction, the slit-edge excited SPPs, and the probe-tip excited SPPs respectively. Figure 5 shows the ray paths of these sources, and their complex electric field amplitudes are described by,

$$\begin{aligned} E_i(x, z) &= E_0 \\ E_{sp_edge}(x, z) &= E_1 e^{i(k_{sp,x}x - k_0 \cos \theta x + k_{sp,z}z + \phi_0)} \\ E_{sp_probe}(x, z) &= E_2 r \sqrt{\frac{d_{probe}}{4\pi x}} e^{i(-2k_{sp,x}x + k_{sp,z}z)}, \text{ for } x > 0 \end{aligned} \quad (2)$$

In Eqn. (2), E_0 , E_1 and E_2 are real valued constants, k_0 is the wave vector of the illumination, θ is the illumination angle with respect to the sample surface, k_{sp} is the SPP wavenumber with components along the x and z directions labeled as $k_{sp,x}$ and $k_{sp,z}$, r is the SPP reflection coefficient for the slit-edge, ϕ_0 is the phase of the slit-edge excited SPPs, and d_{probe} is the effective scattering cross-section of the probe-tip.

E_{sp_probe} contains a phase term $-2k_{sp,x}x$ due to wave reflection from the slit-edge. Equation (2) is strictly valid for positive values of x with the origin of the coordinate system positioned at the edge of the slit. It is assumed that the incident light field and the slit-edge excited SPPs can be approximated as plane waves. The radiated SPPs from local asperities on the sample are assumed to be negligible. The SPP wave vector component $k_{sp,x}$ is obtained from the dispersion relation⁵², $k_{sp,x} = \frac{\omega_0}{c} \sqrt{\frac{\epsilon_m \epsilon_d}{\epsilon_m + \epsilon_d}}$,

where ω_0 and c are the light frequency and phase velocity, ϵ_d and ϵ_m are the electric permittivities of the dielectric (air) and the metal film obtained from the literature⁵³. The amplitude of the near-field scattered by the probe-tip was approximated by $E_{nf}(x, z) \approx \alpha_{eff} E_p(x, z)^{54}$, where α_{eff} is the near-field coupling factor between the probe-tip and the sample, otherwise called the effective polarizability. Thus, the total near-field intensity collected in the far-field is given by $I_{nf} \propto |E_p(x, 0)|^2$. Using the expressions for the complex electric amplitudes stated by Eqns. (1) and (2), I_{nf} is given by,

$$I_{nf} \propto |E_p(x, 0)|^2 = E_0^2 \left[1 + \left(\frac{E_1}{E_0}\right)^2 + \left(\frac{E_2}{E_0}\right)^2 \frac{r^2 d_{probe}}{4\pi x} + 2 \frac{E_1}{E_0} \cos(k_{sp,x}x - k_0 \cos \theta x + \phi_0) + \frac{E_2}{E_0} r \sqrt{\frac{d_{probe}}{\pi x}} \cos(2k_{sp,x}x) + \frac{E_1 E_2}{E_0^2} r \sqrt{\frac{d_{probe}}{\pi x}} \cos[3k_{sp,x}x - k_0 \cos \theta x + \phi_0] \right] \quad (3)$$

- Barnes, W. L., Dereux, A. & Ebbesen, T. W. Surface plasmon subwavelength optics. *Nature* **424**, 824 (2003).
- Gramotnev, D. K. & Bozhevolnyi, S. I. Plasmonics beyond the diffraction limit. *Nat Photonics* **4**, 83 (2010).
- Hecht, B., Bielefeldt, H., Novotny, L., Inouye, Y. & Pohl, D. W. Local excitation, scattering, and interference of surface plasmons. *Phys Rev Lett* **77**, 1889 (1996).
- Nerkararyan, K. V. Superfocusing of a surface polariton in a wedge-like structure. *Phys Lett A* **237**, 103 (1997).
- Fang, N., Lee, H., Sun, C. & Zhang, X. Sub-diffraction-limited optical imaging with a silver superlens. *Science* **308**, 534 (2005).
- Furukawa, H. & Kawata, S. Local field enhancement with an apertureless near-field-microscope probe. *Opt Commun* **148**, 221 (1998).
- Wang, Y., Srituravanich, W., Sun, C. & Zhang, X. Plasmonic near-field scanning probe with high transmission. *Nano Lett* **8**, 3041 (2008).
- Bouhelier, A., Renger, J., Beversluis, M. R. & Novotny, L. Plasmon-coupled tip-enhanced near-field optical microscopy. *J Microsc-Oxford* **210**, 220 (2003).
- Kawata, S., Inouye, Y. & Verma, P. Plasmonics for near-field nano-imaging and superlensing. *Nat Photonics* **3**, 388 (2009).
- Srituravanich, W., Fang, N., Sun, C., Luo, Q. & Zhang, X. Plasmonic nanolithography. *Nano Lett* **4**, 1085 (2004).
- Zeng, B. B., Yang, X. F., Wang, C. T. & Luo, X. G. Plasmonic interference nanolithography with a double-layer planar silver lens structure. *Opt Express* **17**, 16783 (2009).
- Luo, X. G. & Ishihara, T. Surface plasmon resonant interference nanolithography technique. *Appl Phys Lett* **84**, 4780 (2004).

- Kneipp, K. *et al.* Single molecule detection using surface-enhanced Raman scattering (SERS). *Phys Rev Lett* **78**, 1667 (1997).
- Rao, S. *et al.* Single DNA molecule detection in an optical trap using surface-enhanced Raman scattering. *Appl Phys Lett* **96** (2010).
- Nie, S. M. & Emory, S. R. Probing single molecules and single nanoparticles by surface-enhanced Raman scattering. *Science* **275**, 1102 (1997).
- Hayazawa, N., Inouye, Y., Sekkat, Z. & Kawata, S. Near-field Raman scattering enhanced by a metallized tip. *Chem Phys Lett* **335**, 369 (2001).
- Neumann, T., Johansson, M. L., Kambhampati, D. & Knoll, W. Surface-plasmon fluorescence spectroscopy. *Adv Funct Mater* **12**, 575 (2002).
- Yu, F., Persson, B., Lofas, S. & Knoll, W. Attomolar sensitivity in bioassays based on surface plasmon fluorescence spectroscopy. *J Am Chem Soc* **126**, 8902 (2004).
- Liebermann, T. & Knoll, W. Surface-plasmon field-enhanced fluorescence spectroscopy. *Colloid Surface A* **171**, 115 (2000).
- Hubert, C. *et al.* Role of surface plasmon in second harmonic generation from gold nanorods. *Appl Phys Lett* **90**, 181105 (2007).
- Luong, N., Cheng, C. W., Shih, M. H. & Kuang, W. Phase matching for surface plasmon enhanced second harmonic generation in a gold grating slab. *Appl Phys Lett* **100**, 181107 (2012).
- Liu, Z. W. *et al.* Focusing surface plasmons with a plasmonic lens. *Nano Lett* **5**, 1726 (2005).
- Zayats, A. V. & Smolyaninov, I. I. Near-field photonics: surface plasmon polaritons and localized surface plasmons. *J Opt A-Pure Appl Op* **5**, S16 (2003).
- Weeber, J. C. *et al.* Near-field observation of surface plasmon polariton propagation on thin metal stripes. *Phys Rev B* **64**, 045411 (2001).
- Zenhausen, F., Martin, Y. & Wickramasinghe, H. K. Scanning Interferometric Apertureless Microscopy - Optical Imaging at 10 Angstrom Resolution. *Science* **269**, 1083 (1995).
- Hillenbrand, R. & Keilmann, F. Material-specific mapping of metal/semiconductor/dielectric nanosystems at 10 nm resolution by backscattering near-field optical microscopy. *Appl Phys Lett* **80**, 25 (2002).
- Weston, K. D., DeAro, J. A. & Buratto, S. K. Near-field scanning optical microscopy in reflection: A study of far-field collection geometry effects. *Rev Sci Instrum* **67**, 2924 (1996).
- Hosaka, N. & Saiki, T. Near-field fluorescence imaging of single molecules with a resolution in the range of 10 nm. *J Microsc* **202**, 362 (2001).
- Pile, D. F. & Gramotnev, D. K. Adiabatic and nonadiabatic nanofocusing of plasmons by tapered gap plasmon waveguides. *Appl Phys Lett* **89**, 041111 (2006).
- Issa, N. A. & Guckenberger, R. Optical nanofocusing on tapered metallic waveguides. *Plasmonics* **2**, 31 (2007).
- Gramotnev, D. K., Vogel, M. W. & Stockman, M. I. Optimized nonadiabatic nanofocusing of plasmons by tapered metal rods. *J Appl Phys* **104**, 034311 (2008).
- Wang, Y., Reinhard, B. M., Sun, C. & Zhang, X. Particle enhanced plasmonic NSOM. *Proc SPIE* **6642**, 664208 (2007).
- Sanchez, E. J., Krug, J. T. & Xie, X. S. Ion and electron beam assisted growth of nanometric Si_mO_n structures for near-field microscopy. *Rev Sci Instrum* **73**, 3901 (2002).
- Ropers, C. *et al.* Grating-coupling of surface plasmons onto metallic tips: A Nanoconfined Light Source. *Nano Lett* **7**, 2784 (2007).
- Pan, L. *et al.* Maskless plasmonic lithography at 22 nm resolution. *Sci Rep* **1**, 175 (2011).
- Stockman, M. I. Nanofocusing of optical energy in tapered plasmonic waveguides. *Phys Rev Lett* **93**, 137404 (2004).
- Babadjanyan, A. J., Margaryan, N. L. & Nerkararyan, K. V. Superfocusing of surface polaritons in the conical structure. *J Appl Phys* **87**, 3785 (2000).
- Verhagen, E., Kuipers, L. & Polman, A. Enhanced nonlinear optical effects with a tapered plasmonic waveguide. *Nano Lett* **7**, 334 (2007).
- Verhagen, E., Spasenović, M., Polman, A. & Kuipers, L. Nanowire plasmon excitation by adiabatic mode transformation. *Phys Rev Lett* **102**, 203904 (2009).
- Lindquist, N. C., Nagpal, P., Lesuffleur, A., Norris, D. J. & Oh, S.-H. Three-dimensional plasmonic nanofocusing. *Nano Lett* **10**, 1369 (2010).
- Verhagen, E., Kuipers, L. & Polman, A. Plasmonic nanofocusing in a dielectric wedge. *Nano Lett* **10**, 3665 (2010).
- Berweger, S., Atkin, J. M., Olmon, R. L. & Raschke, M. B. Light on the tip of a needle: plasmonic nanofocusing for spectroscopy on the nanoscale. *J Phys Chem Lett* **3**, 945 (2012).
- Sadiq, D. *et al.* Adiabatic nanofocusing scattering-type optical nanoscopy of individual gold nanoparticles. *Nano Lett* **11**, 1609 (2011).
- Vedantam, S. *et al.* A plasmonic dimple lens for nanoscale focusing of light. *Nano Lett* **9**, 3447 (2009).
- Ocelic, N., Huber, A. & Hillenbrand, R. Pseudoheterodyne detection for background-free near-field spectroscopy. *Appl Phys Lett* **89**, 101124 (2006).
- Ahn, P., Zhang, Z., Sun, C. & Balogun, O. Ultrasonic near-field optical microscopy using a plasmonic nanofocusing probe. *J Appl Phys* **113**, 234903 (2013).
- Srituravanich, W. *et al.* Flying plasmonic lens in the near field for high-speed nanolithography. *Nat Nanotechnol* **3**, 733 (2008).
- Huber, A., Ocelic, N., Kazantsev, D. & Hillenbrand, R. Near-field imaging of mid-infrared surface phonon polariton propagation. *Appl Phys Lett* **87**, 081103 (2005).
- Huber, A. J., Ocelic, N. & Hillenbrand, R. Local excitation and interference of surface phonon polaritons studied by near-field infrared microscopy. *J Microsc* **229**, 389 (2008).



50. Knoll, B. & Keilmann, F. Enhanced dielectric contrast in scattering-type scanning near-field optical microscopy. *Opt Commun* **182**, 321 (2000).
51. Aubert, S. *et al.* Analysis of the interferometric effect of the background light in apertureless scanning near-field optical microscopy. *J Opt Soc Am B* **20**, 2117 (2003).
52. Sambles, J. R., Bradbery, G. W. & Yang, F. Z. Optical excitation of surface-plasmons: an introduction. *Contemp Phys* **32**, 173 (1991).
53. Palik, E. D. Handbook of optical constants (A). *J. Opt. Soc. Am. A* **1**, 1297 (1984).
54. Hillenbrand, R., Knoll, B. & Keilmann, F. Pure optical contrast in scattering-type scanning near-field microscopy. *J Microsc* **202**, 77 (2001).

Acknowledgments

The authors acknowledge the support of the National Science Foundation under Grant No. CMMI-1031574, CMMI-0955195, and CMMI-0751621.

Author contributions

C.S. and O.B. initiated and supervised the project. Z.Z. and B.D. performed the numerical simulation of plasmonic nanofocusing probe and established the analytical model. P.A. characterized the performance of plasmonic nanofocusing probe and conducted p-NSOM imaging. B.D., C.S. and O.B. provided guidance on theory and measurements. All authors discussed the results and contributed to the manuscript.

Additional information

Competing financial interests: The authors declare no competing financial interests.

How to cite this article: Zhang, Z., Ahn, P., Dong, B., Balogun, O. & Sun, C. Quantitative Imaging of Rapidly Decaying Evanescent Fields Using Plasmonic Near-Field Scanning Optical Microscopy. *Sci. Rep.* **3**, 2803; DOI:10.1038/srep02803 (2013).



This work is licensed under a Creative Commons Attribution-NonCommercial-NoDerivs 3.0 Unported license. To view a copy of this license, visit <http://creativecommons.org/licenses/by-nc-nd/3.0>